ICAST2015: 26th International Conference on Adaptive Structures and Technologies
October 14-16th, 2015, Kobe, Japan

ICAST2015 #002

Generation of a Shock Control Bump by Pressurized Chambers

Markus Kintscher[1*], Nuno Alves de Sousa[2*], Hans Peter Monner[1], Martin Wiedemann,[1]

[1] Department of Adaptronics, DLR Institute of Composite Structures and Adaptronics, Braunschweig, Germany.
[2] Instituto Superior Técnico, Universidade de Lisboa, Portugal.

Abstract

In the design of a new generation of eco-efficient aircrafts, fuel reduction is the number one objective. To increase the efficiency of the next generation aircraft, disruptive technologies are under investigation to achieve a significant benefit and advantage in the market. Such technologies often mentioned as game changer technologies like for example laminar flows are under investigation since decades and have not yet reached a technology readiness level suitable for serial production of large passenger aircraft. Besides laminar flow and other game-changer technologies, there are technologies like for example variable camber and shock control, which offer less improvement in efficiency compared for example to laminar flow, but which are easier to get developed to the needed technology readiness level since only small changes in system architecture and/or the structural layout are necessary. Therefore in this paper a structural concept for an adaptive spoiler shock control bump is presented. The objective of the shock control bump is to spread a single transonic shock which causes a significant drag increase into several smaller shocks with less drag penalty. Since the shock bump performance depends on various parameters and flow conditions like height, density, temperature, flow velocity, etc. the optimal shock position and height is changing during flight. Therefore, a shock control bump concept which is able to adapt the bump to the varying flight conditions is presented. A simplified analytical model for the structure is used in the framework of an optimization module to investigate the interdependencies of structural parameters and actuation parameters for the accurate approximation of given aerodynamic target shapes. An outlook is given on the design issues for a 3D design of the pressure actuated adaptive bump spoiler concept.

Keywords: Shock control bump; wave drag minimization; morphing spoiler; pressure actuated adaptive structure; structural optimization.

* markus.kintscher@dlr.de
nunoalvesdesousa@me.com

1. INTRODUCTION

The reduction of DOC's and the improvement of mission flexibility by incremental improvements is a strategic key issue in the development of the next generation aircraft. For the enhancement of the performance in off-design conditions the adaptation of the wings geometry to changing flight conditions has large potential. There are several performance-enhancing technologies as identified by Schrauf et al.[1] which are under investigation (fig.1). Besides large scale morphing technologies, with the objective to adapt the complete wing as described by Smith[3] on an experimental F-111 fighter, it seems more feasible to adapt the airfoil geometry by focusing on individual movables like the leading edge, flap or the spoiler. Adaptive wing devices as for example a smart droop nose [2] or a smart flap trailing edge can contribute to a drag reduction of lift induced drag and viscous drag as well.

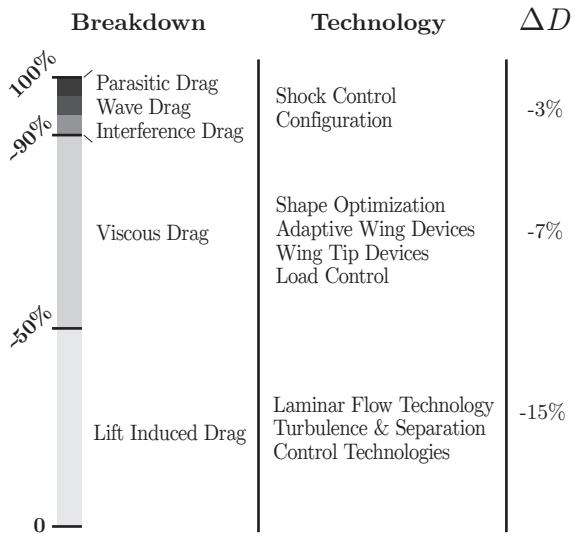

Figure 1: Drag breakdown of transport aircraft in cruise including technologies for drag reduction by Schrauf et al.[1] and estimated potential drag reduction (ΔD)

The most effective approach for the reduction of wave drag is the application of SCBs, according to the EUROSHOCK-program [4] as proposed by Ashill et. al [5] 1992. The control of the transonic shock especially for variable camber (VC) application is a promising concept for wave drag reduction. In transonic flight supersonic regions and shock waves are generated when exceeding the critical Mach number. These increase the entropy while the total pressure decreases. The effect is wave drag which can be reduced by the application of shock control bumps to significantly reduce the shock strength.

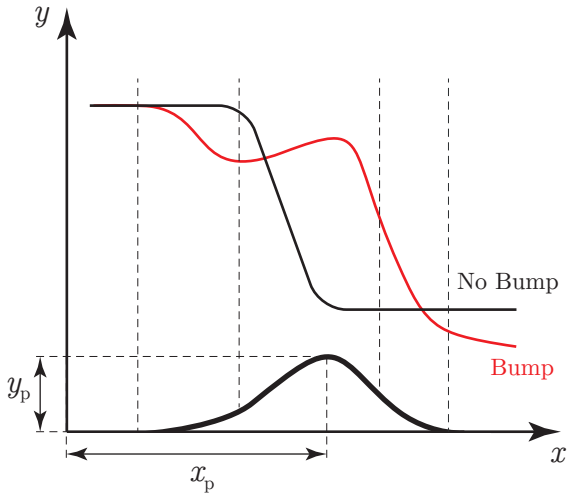

Figure 2: Definition of geometrical key parameters of a shock control bump (SCB)

To do so, a bump must be formed in the region of the shock as depicted in Figure 2. The shock position is located on the rising slope of the bump to induce isentropic compression waves and a pre-shock which reduces the Mach number in front of the main shock. From parametric investigations of Knauer [6] and Dargel [7-8] we know that the potential for drag reduction by the application of shock control bumps (SCBs) depends strongly on the correct bump height y_p and the position x_p of the bump peak. The bump height depends on the actual flight conditions and the airfoil geometry but can be estimated to be within about 0.5 percent of local chord length. Compared to the bump height and position, the detailed bump shape like ramps, polynomials and sinusoidal curves does not have a very strong effect on the bump effectiveness.

2. STRUCTURAL CONCEPT, MODEL AND OPTIMIZATION

For the exploitation of the full potential of the SCB/VC technology, an active system must be developed to be able to adapt the bump position and height to changing flight conditions. While there are numerous publications dealing with the aerodynamic design of SCBs, the structural realization of such a structure-system combination is still a key challenge. Since the shock control bump is located at the chord position of the wings trailing edge and spoilers, the available design space is extremely limited. The main drivers for a concept selection are therefore a compact design, a lightweight structure and a simple and low complexity mechanism for the deployment of the bump. Concepts for structural realization have been compared by Pritschow [9] while concepts using SMA actuated deformation have been realized and tested by Wadehn [10] and Bein [11].

2.1 Concept

According to the above mentioned design drivers a concept with pressurized chambers is selected as pioneering technology combining the key requirements. Using pressure for actuation was also proposed by Bein in [11] as an alternative actuation concept to the application of shape memory alloys. The deployment of a SCB by pressure and its adaptation to changing flight conditions is realized by differential pressurization of chambers in the spoiler body (fig.3).

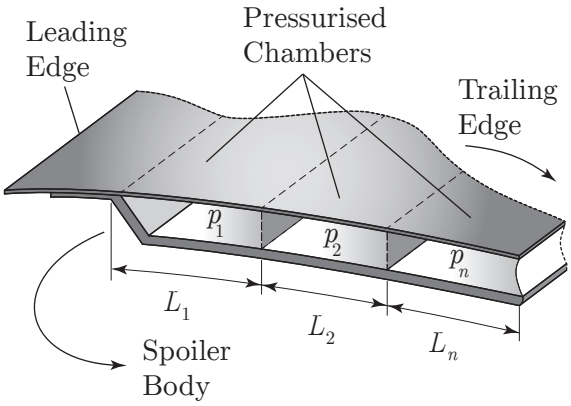

Figure 3: Concept of pressurized chambers for an adaptive spoiler shock control bump

Within the concept the overall structural stiffness is given by a conventional "rigid" spoiler lower body, while the flexibility for realization of a SCB is given by thinner upper spoiler cover. Pressurized chambers are formed by separating walls which can be realized for example by stringers with a cross-sectional shape allowing for deformation in direction of the chamber height which at the same time can serve as standard longitudinal stiffeners in span direction.

2.2 Analytical Model & Optimization

A simplified spoiler model is proposed to expedite the pre-design stage and to cope with the necessity of defining a set of design variables which offers enough degrees of freedom to generate the required bump shapes.

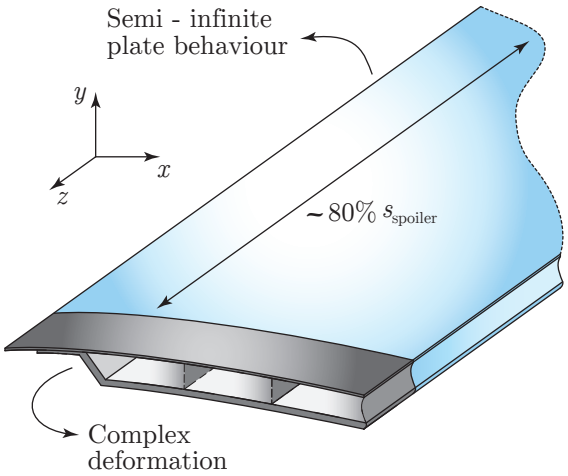

Figure 4: Different deformation behaviours

The upper spoiler skin is modelled as a transversely loaded plate while the main lower body

is assumed to be comparably much stiffer. If the spoiler edges are free at both ends (*i.e.* the upper skin tips), it is then possible to identify two regions that exhibit different deformation behaviours. Figure 4 shows that near both spoiler tips (depicted in grey) there is a relatively small region where the deformation along the z-axis is complex.

The inner blue region, where the tip deformation has little influence, deforms almost uniformly along z. This can be called the "effective bump region" (EBR), and the plate is idealized as infinite along the span direction.

For transversely loaded Kirchhoff plates and an isotropic and homogeneous material, the deformation along y is given by

$$\frac{\partial^4 v}{\partial x^4} + 2\frac{\partial^4 v}{\partial x^2 \partial z^2} + \frac{\partial^4 v}{\partial z^4} = \frac{p}{D} \tag{1}$$

where p is the transverse loading. D is defined as follows

$$D = \frac{EH^3}{12(1-\nu^2)} \tag{2}$$

where E is the Young's Modulus, ν is the Poission coefficient and H is the half-plate thickness $H = h/2$.

Additionally, for the blue region $\partial/\partial z = 0$ and eq.1 becomes

$$E^* I \frac{\mathrm{d}v^4}{\mathrm{d}x^4} = p \tag{3}$$

where

$$E^* = \frac{E}{1-\nu^2} \quad \text{and} \quad I \coloneqq \frac{H^3}{12} \tag{4}$$

Showing that for the blue region it is possible to implement a beam-like solution process where the upper skin of each chamber is modelled as a beam segment per unit span with a scaled Young's Modulus E^*.

Figure 5 shows the upper surface of the wing idealized as a series of beams which are actuated by the pressurized chambers inside the spoiler. A spring is used to model the interface between different bays whose pressure is kept constant.

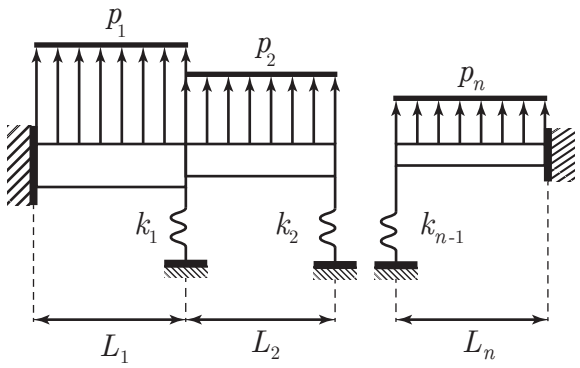

Figure 5: Simplified 2D model

The model is then used in an optimization environment where the desired bump shapes are fed to the optimization algorithm through an objective function as target shapes in order to find the optimized design parameters that minimize the difference between the target shape (*i.e.* the desired bump) and the optimized shape. The design parameters include:

- α_i - the relative position of each spring as a percentage of the total spoiler chord. This is then used to compute the length L_i of each chamber;
- t_i - the thickness of the upper skin of each chamber;
- k_i - the spring constant;
- p_i - the pressure inside each chamber.

It is also possible to choose the number of beam segments (*i.e.*: the number of pressurized chambers) which is directly related to the overall design complexity.

2.2.1 Structural Module

A structural model is developed based on the analytic element method (AEM) approach as described by Policarpo et al.[12]. This allows for a structural solver which is both accurate and efficient.

Since the pressure inside each chamber is assumed to be uniform

$$v_i(x) = \frac{p_i}{24H_i}x^2 + C_1^i x^3 + C_2^i x^2 + C_3^i + xC_4^i \quad (5)$$

where $H_i = E_i^* I_i$ is the flexural rigidity of beam i and C^i are the set of beam constants to be determined using the boundary conditions. The loads on the left (I), and right (J) nodes are respectively given in terms of shear force (V) and bending moment (M) by

$$\begin{Bmatrix} F_i^I \\ M_i^I \\ F_i^J \\ M_i^J \end{Bmatrix} = \begin{Bmatrix} -V(x=0) \\ -M(x=0) \\ V(x=L_i) \\ M(x=L_i) \end{Bmatrix} \quad (6)$$

Similarly, it is possible to write the nodal degrees of freedom $\{p\}$ (*i.e.* the nodal deflections and rotations) as a function of the C^i analytic constants. Noting that $\theta(x) = \mathrm{d}v/\mathrm{d}x$,

$$\begin{Bmatrix} v_i^I \\ \theta_i^I \\ v_i^J \\ \theta_i^J \end{Bmatrix} = \begin{Bmatrix} v(x=0) \\ v'(x=0) \\ v(x=L_i) \\ v'(x=L_i) \end{Bmatrix} \quad (7)$$

Using the shear force and bending moment definitions and eq.5 it is possible to rewrite eq.6 and eq.7 as follows,

$$\{F\} = [B]\{c\} + \{q\} \quad (8)$$

$$\{p\} = [C]\{c\} + \{g\} \quad (9)$$

where matrices $[B]$ and $[C]$ as well as vectors $\{q\}$ and $\{g\}$ are only functions of the design parameters. Solving equations 8 and 9 simultaneously holds a familiar FEM representation

$$[K]\{p\} = \{F\} + \{f\} \quad (10)$$

Where $[K]$ is the stiffness matrix, $\{F\}$ and $\{f\}$ are the nodal and distributed loads, respectively. The relation with the original matrices is given by

$$\begin{cases} [K] & = [B][C]^{-1}\{p\} \\ \{f\} & = [B][C]^{-1}\{g\} - \{g\} \end{cases} \quad (11)$$

Therefore, the solver implementation is very similar to the FEM approach for both assembly and solving algorithms.

The AEM maximizes accuracy because it retrieves the exact solution, while the FEM would retrieve the exact nodal displacements but underestimate the deflection between the nodes for a given distributed loading, leading to an underestimation of the required pressure. The AEM also maximizes speed because it minimizes the number of elements required to describe each pressurized chamber.

Reducing the overall number of elements also contributes to the efficiency of the optimizer algorithm.

2.2.2 Optimization Module

The optimization module uses the simplex search method of Lagarias et al.[13] and includes variable transformation to address bound constraints for the optimization parameters. This can be used to define both design criteria constraints (*e.g.*: minimum beam thickness and length) as well as constraints imposed by the pressure limits inside each chamber.

The initial set-up requires the user to input a base shape for the "unbumped" spoiler, a target shape, the number of pressurized chambers (*i.e.*: number of beams). A set of constraints for the optimization parameters may be provided as well.

Eq.12 shows the implementation of the objective function.

$$r_j = \max\left(\frac{\left|\overrightarrow{QP_k^j}\cdot\mathbf{n}\right|}{\|\mathbf{n}\|}\right) \quad (12)$$

The minimization objective is r_j and it represents the maximum difference between the current j-iteration deformed shape and the target shape. The deviation is computed by sampling a series of $P_k^j(x_k, y_k)$ points along the shape of the current iteration ($k = 1, 2, ...$ n.º of sample points) and then finding the minimum distance from each of these points to a generic $Q_(x, y)$ point along the target

shape.

Fig.6 shows how the structural and optimization modules are integrated into the design algorithm.

The base and target shapes are first loaded and the user inputs the number of pressurized chambers. Each chamber is associated with a series of new optimization parameters. Adding chambers has therefore a very significant impact on the problem complexity. Moreover, increasing the number of optimization parameters has a disproportional effect on the number of calculations the optimizer must perform and consequently leads to a rapid growth of the algorithm runtime.

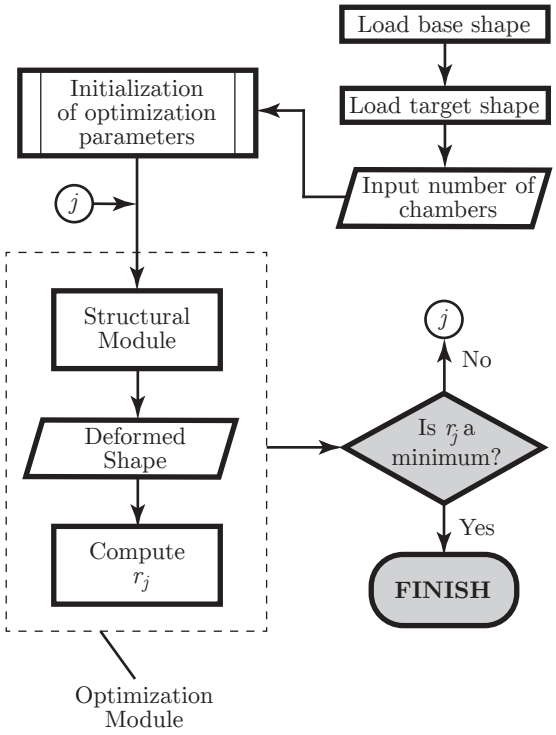

Figure 6: Flow diagram for the design algorithm

2.2.3 Target Shapes

As shown by Sommerer et all.[14] the position of the bump peak plays an important role for the drag reduction but the exact bump shape doesn't. This means that there is freedom to generate the target shapes in a way that is more efficient (*i.e.* requires less pressure to achieved the desired peak position) while still respecting mandatory shape constrains imposed by the nature of the structure (*i.e.* clamped leading and trailing edges). Therefore, if care is not taken while generating those shapes, a beam model with physical background might not able to approximate the given target shape, or it might do so using an excessive actuation pressure.

The target shapes are generated using cubic splines that interpolate the desired peak position and ensure compatibility with the clamped leading and trailing edges.

The next figure shows the typical "overshoot" that happens on the optimized shape when the target shapes are generated using a cubic spline containing only the peak position P and both leading (O) and trailing (L) edges. The target shape is very asymmetric around the peak position and the asymmetry increases as the peak moves towards the leading or trailing edges. Therefore, the peak of the optimized shape tends to deviate from point P so that it is possible to minimize the maximum difference between the curves.

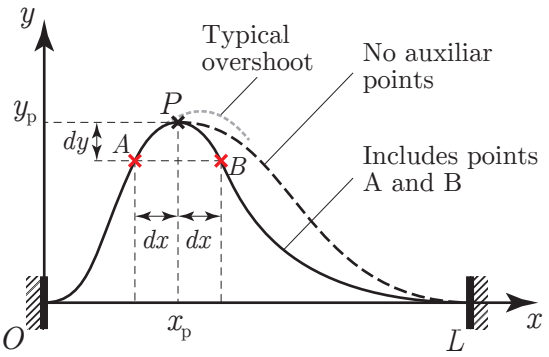

Figure 7: Bump shape geometry

The solution is enforcing some degree of local symmetry around point P using the auxiliary points $A(x_p-dx, y_p-dy)$ and $B(x_p+dx, y_p-dy)$. Values of dx and dy that better approximate the actual physical behaviour will then have to be deter-

mined.

When interpolating point B, the slope is averaged using x_p

$$\left.\frac{dy}{dx}\right|_B = \frac{x_p\left(-\left.\frac{dy}{dx}\right|_A\right) + \left(\frac{L_x}{2} - x_p\right) m_{\overline{BL}}}{\frac{L_x}{2}} \quad (13)$$

so that when $x_p = L/2$ the curve is perfectly symmetric (*i.e.* $dy/dx|_A = -dy/dx|_B$). The case $x_p = 0$ corresponds to the limit when B would be exactly vertical to O and $dy/dx|_B = m_{\overline{BL}}$, where $m_{\overline{BL}}$ is the slope of the straight line connecting those two points.

After generating the bump shape as in fig.7, the actual target shape is computed by adding the bump shape to the base spoiler profile in the direction perpendicular to the upper spoiler skin.

3. RESULTS

3.1 Target Shapes

Figure 8 illustrates the impact that the target shape has on the optimized peak position of a simple two chamber spoiler design with 0,8 m of chord length (c_{sp}) and a fibreglass skin. Different target shapes that include the same peak position $x_p = 0.35c_{\text{sp}}$, $y_p = 0.05c_{\text{sp}}$ are compared. The curves have been vertically spaced for visualization purposes only.

Target shape A uses no auxiliary points and the peak "overshoot" is the highest in both x and y directions. The other curves include auxiliary points with fixed $dy = 0.10y_p$ and varying values of dx.

Target B and C represent two extreme cases. Curve B has a large value of dx and the target peak radius is too large. The peak of the optimized shape has too much vertical displacement. Curve C has a small dx which means the target peak radius is too small and the optimized shape has too little vertical displacement. However, it is clear that adding the auxiliary points improves greatly the horizontal positioning of the peak in both cases because of the resultant local symmetry enforcement.

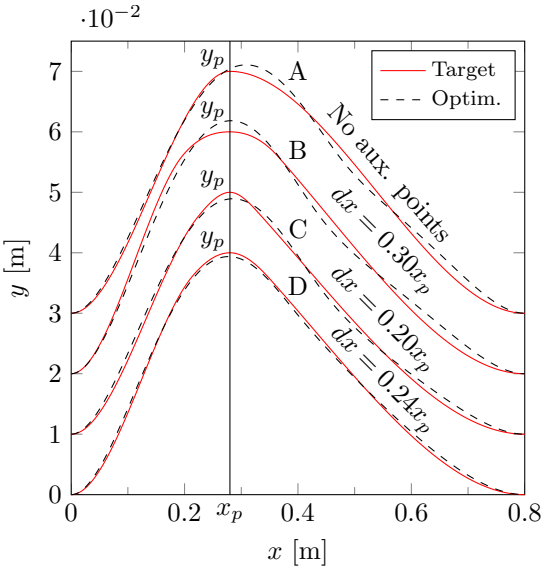

Figure 8: Effect of parameters dx and dy

Curve D shows that after proper adjustment of the values dx and dy it is possible to generate target shapes that not only meet the design constraints, but are also more easily realizable by the physical model.

3.2 Deformation Envelope

Different aircraft have different aerodynamic requirements regarding the bump shapes. Moreover, for a given aircraft, the optimal bump shape also varies under different flight conditions. This means that there is the need for an envelope of spoiler bump deformations. In this section, a simple flat spoiler is considered and a range of bump shapes are generated by varying the peak position along the chord of the spoiler.

Figure 9 shows the deformation envelope for a group of peak positions ranging from 20% to 45% of the total chord length while the peak height is kept constant and equal to 5% of the chord length. The dashed vertical lines represent the optimal position of the two chamber interface for each target.

The deformation envelope can be completed with an actuation envelope. The actuation envelope is computed by plotting the maximum chamber pressure against the peak position. Figure 10 shows the actuation envelope that results from the deformation envelope presented in fig.9 for the two chamber design.

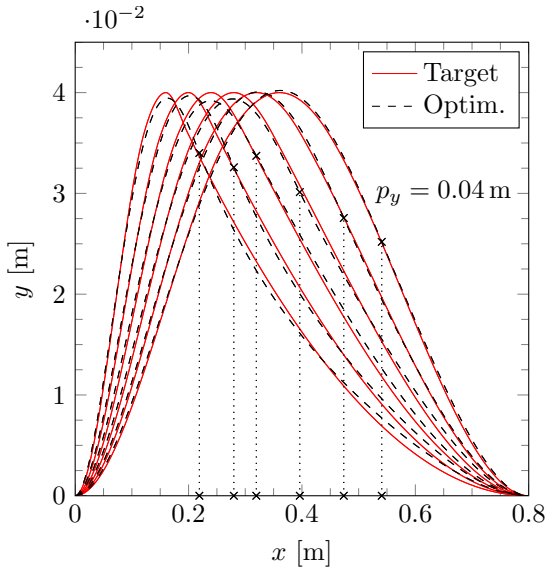

Figure 9: Typical deformation envelope

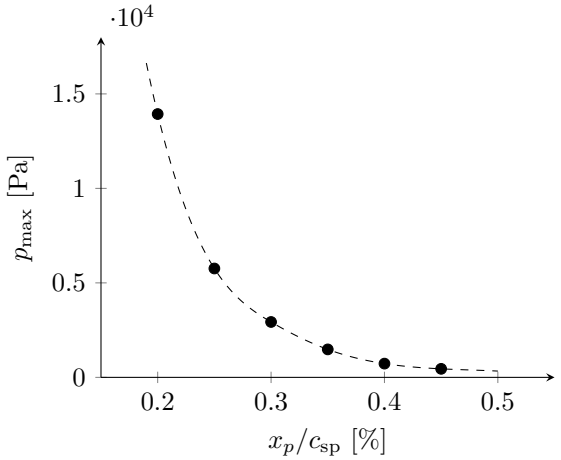

Figure 10: Typical actuation envelope

As a simple flat spoiler was considered for the "clean configuration", the minimum actuation pressure happens when the peak position is located symmetrically in the middle of the plate. As the peak moves towards the leading or trailing edges, the pressure starts increasing disproportionately as a consequence of the greater deformation level required for such configurations. The actuation envelope is therefore symmetric to $x_p/c_{\mathrm{sp}} = 0.5$.

It is clear that the actuation pressure can vary considerably as the optimal peak position changes due to aerodynamic reasons (*e.g.* change in flight conditions and/or aircraft weight). Which draws attention to the fact that, once a chamber configuration is chosen, generating bumps in off-design conditions can become extremely inefficient. This means that a detailed aerodynamic study must be carried out for each specific aircraft in order to ensure that the required deformation envelope (determined by the aerodynamics) is located in the most favourable region of the actuation envelope (to increase structural efficiency).

For more complex "clean configurations" (*i.e.* spoilers with curved base shapes) and complex aerodynamic requirements that leads to challenging deformation requirements and it might be necessary to use a tapered upper spoiler skin in order to cope with the fact that the chamber configuration is fixed in the final design.

3.3 Number of Chambers

The number of pressurized chambers affects directly the weight and complexity of the spoiler structure.

Therefore in this section, the influence of the number of chambers on the spoiler efficiency is investigated. The same spoiler is used to generate a deformation envelope identical to the one in fig.9 using now three chambers.

Figure 11 shows the actuation envelope for the three chamber configuration. The maximum actuation pressure is no longer symmetric in respect to the middle of the spoiler. Nevertheless, and as previously, as the peak position moves towards both the leading and trailing edges, the required maximum pressure increases significantly.

To better assess the effect of an additional chamber, figure 12 shows the relative difference between maximum chamber pressures for the two configurations in study.

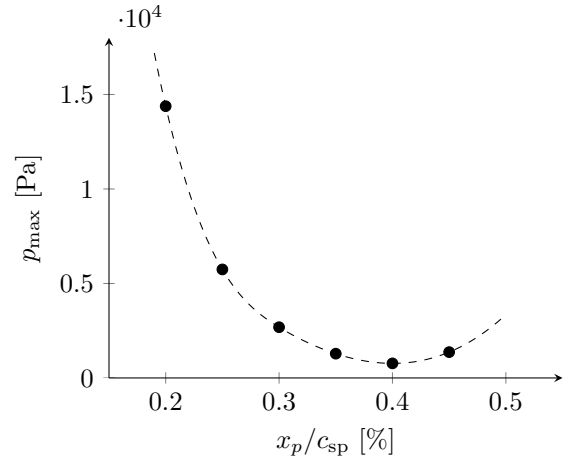

Figure 11: Actuation envelope for the three chamber spoiler.

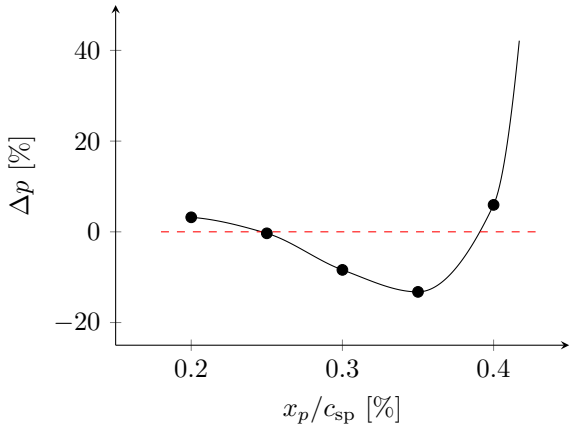

Figure 12: Pressure variation

It is possible to verify that, even though there is a loss of structural efficiency for the outermost regions of the spoiler, the inner region actually benefits from a lowering of up to 13% of the maximum pressure compared to the two chamber configuration. For the current spoiler, adding extra chambers wouldn't contribute to a substantial decrease of the actuation pressure.

Figure 13 shows the pressure history during the optimisation process for point $x_p/c_{\text{sp}} = 0.35$ of fig. 12 where the 3 chamber design lowers most effectively the actuation pressure. The spoiler with two chambers is depicted in black while the three chamber configuration is shown in red. The chamber number increases from leading to trailing edge.

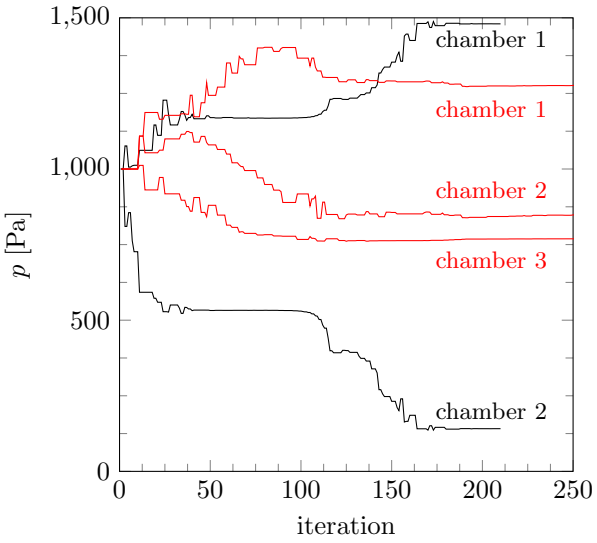

Figure 13: Pressure during the optimization for a peak position of $x_p/c_{\text{sp}} = 0.35$

The region of the actuation envelope where the three chamber configuration allows for a reduction of the maximum actuation pressure behaves as fig.13 and fig.14. Adding another chamber within the innermost region of the spoiler allows the reduction of the maximum actuation pressure (i.e. pressure in chamber 1 is lower for the three chamber design). The pressure in the remaining chambers increases.

Figure 14 shows that when a chamber is added within the innermost region of the spoiler, its end moves to the trailing edge. This facilitates generating the peak shape at lower pressure levels.

However, as a trade-off, because of the added flexural rigidity introduced by an additional interface between new chambers and the greater length of the first chamber, the local slope at the intersection of chambers 1 and 2 is higher. Chambers 2 and

3 are therefore used to recover the trailing edge geometry at the cost of an increased actuation pressure in those chambers because their interface contributes to the upper skin flexural rigidity and can be interpreted as "a cost of adding extra chambers".

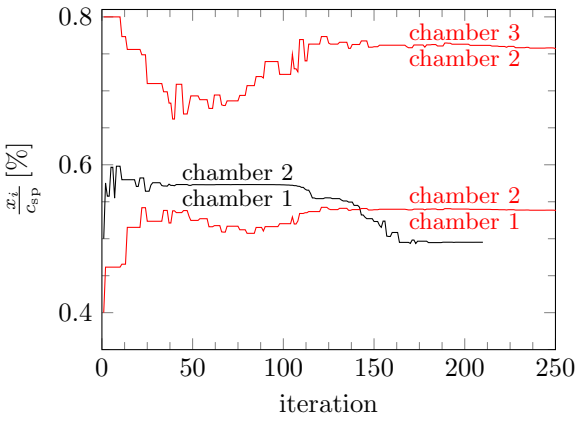

Figure 14: Chamber positioning

For more complex base shapes, and depending on the specific aerodynamic requirements, an assessment of the increased structural complexity that arises from additional chambers should always be carried out first. Specially if the deformation envelope needs to include some peak positions in the outermost regions.

3.4 Spoiler Ends

The design of the spoiler ends has a great impact on the structure performance and its capacity not only to conform to the desired peak position, but also to maintain an aerodynamically acceptable shape. In this section, three different designs for the spoiler ends are considered: a spoiler with open ends (and thus free tips); a spoiler with fixed ends and a spoiler whose ends have been closed using a 1 mm thin fibreglass plate like the upper spoiler skin.

The results are computed using a commercial FEM code and a complete 3D spoiler model. Fig.15 shows the deformation for each design: the dashed curves represent the deformation of the spoiler tips (*i.e.* upper skin edge at both spoiler ends) and the solid lines show the deformation in the middle of the spoiler.

For the spoiler configuration with free ends, the bump profiles on the spoiler tips and midplane present little variation. Moreover, the midplane bump is exactly coincident with the bump shape predicted by the structural solver that was developed. The full 3D model shows that the outermost region of the spoiler experiences some additional deformation, but for the innermost region, there is good concordance between the full 3D model and the simplified semi-infinite plate model.

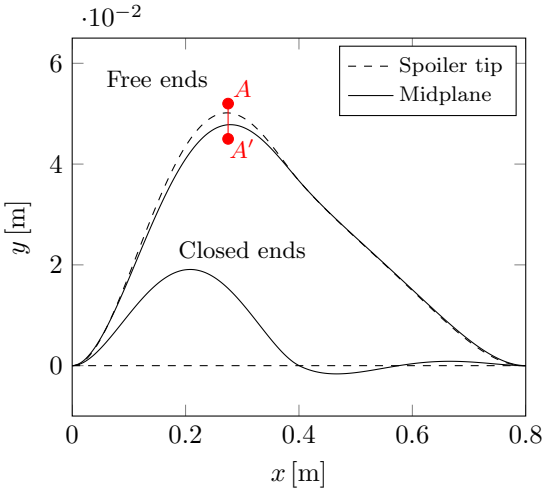

Figure 15: Pressure during the optimization

The designs with closed and fixed ends are much stiffer. Both designs present identical deformations and for that reason only the closed end variant is depicted in fig.15. The additional stiffness introduced by the closing plates has a dramatic effect on the deformation of the spoiler tip bump which now behaves as if it were fixed. The inner region is also greatly affected: not only is the deformation much lower than desired, but the peak position on the x axis is considerably different. The bump profile is also completely altered and a "wavy" region near the spoiler trailing edge appears.

Figure 16 presents the span-wise evolution of

the peak deflection obtained by inspecting the upper skin deformation along a plane AA' coincident with the peak position as shown in figure 15. The same was done along the fixed and closed end designs. The latter have almost the same span-wise deformation except for a region near the ends where the spoiler with the closing plates presents a slightly larger deformation. In any case, such configurations lead to completely different solutions, showing that the structural model developed can only be used for accurate predictions if the spoiler has free ends. Again, the red line in figure 15 shows that there is indeed a considerably larger region ("the effective bump region") where the current model provides accurate predictions and can be used as a useful design tool.

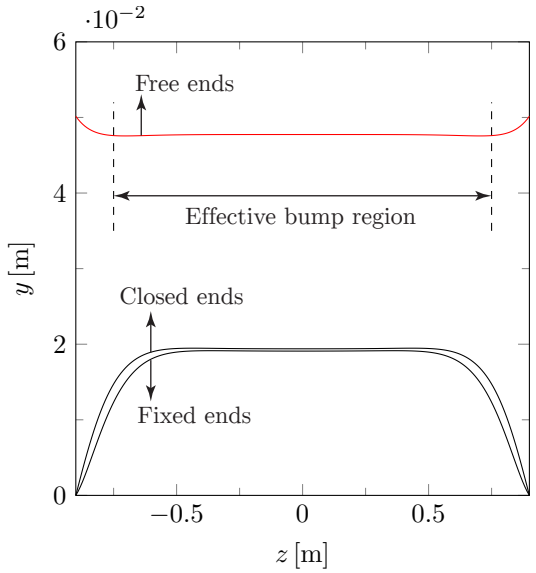

Figure 16: Span-wise peak deformation

On a final note, it should be mentioned that closing or fixing the spoiler ends increases the bump deformation complexity considerably and leads inevitably to a completely 3-dimensional problem where simplified models can hardly be implemented. Furthermore, even if the actuation pressure is increased in order to reach the desired peak deflection, the deformation would, as mentioned, lead to a "wavy" region near the trailing edge that presumably has a very negative effect on the aerodynamics. Therefore, the free end concept seems to be the most promising alternative as it provides a large region where the bump shape is maintained uniform using lowest actuation pressure possible and avoiding complex and aerodynamically unfavorable span-wise deformations.

4. CONCLUDING REMARKS

A structural concept of pressurized chambers is presented in this study for the realization of an adaptive spoiler shock control bump. Using a simplified 2D parametric model the influence of selected design parameters is investigated. Depending on the geometry of pressurized chambers the effect on the actuation pressure is studied. Furthermore, the effect of an increasing number of chambers on the actuation pressure and the chamber design is investigated. The deployment of the bump for various designs of the spoiler ends closing is presented.

Since the peak position (chord-wise location and deflection of the bump peak) is the driving aerodynamic parameter, a method for generating "easily realizable" bump shapes (from a structural standpoint) is proposed.

The concept suggested has enough freedom to conform to a wide range of bump shapes even for a simple 2 chamber design. It has been shown that increasing the number of chambers can lead to a reduction of the actuation pressure, but since each chamber interface contributes to an added flexural rigidity, this effect can only be used within a limited region of peak positions and up to a maximum number of chambers that varies according to the different spoiler base shapes.

The type of closing of the spoiler ends has been shown to have both a strong impact on the ability of the structure to conform to the desired peak position and also on the quality of the entire bump target shape.

ACKNOWLEDGEMENTS

The work is funded by the 5^{th} Federal Aeronautical Research Program (LUFO V) by the Federal Ministry of Economic Affairs and Energy (BMWi) in the project LDAinOP, FkZ: 20A1302B.

REFERENCES

1. SCHRAUF G., GÖLLING, B., WOOD, N. *Key Aerodynamic Technologies for Aircraft Performance Improvement*. "KATnet- 5th Community Aeronautical Days 2006" Vienna, Austria, 19-21st June 2006
2. KINTSCHER, M. and WIEDEMANN, M. *Design of a smart leading edge device*. In: Adaptive, Tolerant and Efficient Composite Structures Springer. Pages 381-390. ISBN 978 3 642 29189 0.
3. SMITH, W. J., LOCK, W.W. *Variable Camber System Integration and Operational Performance of the AFTI/F-111 Mission Adaptive Wing*. "NASA Technical Memorandum 4370", 1992
4. STANEWSKI, E. *A Euroshock I and II: A survey*. "Proceedings IUTAM Symposium on Mechanics of Passive and Active Flow Control", 7–11 September, 1998, Göttingen, Germany, pp 35– 42. Kluwer Academic Publishers, 1998.
5. ASHILL, W. J., LOCK, W.W. *A novel technique for controlling shock strength of laminar-flow aerofoil sections*. "Proceedings 1st European Forum on Laminar Flow Technology March 16-18th, 1992", pp 175–183. DGLR, AAAF, RAeS, Hamburg, Germany, 1992 *Acta Astronautica*, Vol.12, No.7/8, 1985, pp. 599-607.
6. KNAUER, A, *Die Leistungsverbesserung transsonischer Profile durch Konturmodifikationen im Stoßbereich*. PhD thesis, DLR, 1998
7. DARGEL G. *Widerstandsreduktion durch Stoßkontrolle mit adaptiver Hautstruktur: Shock Control Bump*. "Proceedings DGLR" Jahrestagung, 1998
8. DARGEL G., ARCHAMBAUDJ. P. *Assessment of the capability of drag reduction of the shock control device sc bump on airfoil flows and application aspects on wing*. "Proceedings IUTAM Symposium on Mechanics of Passive and Active Flow Control 7–11th September, 1998, Göttingen, Germany" pp 57–62. Kluwer Academic Publishers, 1998
9. PRITSCHOW G., WADEHN W. and KEHL G. *Shape adaptation of fixed wing aircraft by shape memory alloys Proceedings of the 7^{th} International Conference on New Actuators*. "Proceedings of the 7th International Conference on New Actuators", Actuator 2000 1012 June, 2000, Bremen, Germany, 2000.
10. WADEHN W., SOMMERER A., LUTZ T., FOKIN D., PRITSCHOW G., WAGNER *S. Structural Concepts and aerodynamic design of shock control bumps*. "Proceedings of the International Council of the Aeronautical Sciences", 23^{rd} Congress of Internation Council of the Aeronautical Sciencies, 8-13 September 2002, Toronto Canada, 2002
11. BEIN T., HANSELKA H. and BREITBACH E. *An adaptive spoiler to control the transonic shock*. "Journal of Smart Mater", Struct. 9, 141148, 2000.
12. POLICARPO, H., NEVES, M.M *Using Symbolic Computation for Teaching Structural Mechanics I: Frames*. "CSEI2012 – Conferência Nacional sobre Computação Simbólica no Ensino e na Investigação", Lisboa, 2-3 Abril de 2012
13. LAGARIAS, J.C., REEDS J. A., WRIGHT M. H., WRIGHT P. E., *Convergence Properties of the Nelder-Mead Simplex Method in Low Dimensions*. "SIAM Journal of Optimization", Vol. 9 Number 1, pp. 112-147, 1998
14. SOMMERER, A., LUTZ, T., WAGNER, S. *Numerical Optimisation of Adaptive Transonic Airfoils with Variable Camber*. "ICAS 2000 Congress", Number 2111, pp. 1-10, 2000